Three dimensional localization of unintentional oxygen impurities in gallium nitride

Electronic Supplementary Information

Paweł Piotr Michałowski,* Sebastian Złotnik and Mariusz Rudziński
Łukasiewicz Research Network-Institute of Electronic Materials Technology
Wólczyńska 133, 01-919 Warsaw, Poland; E-mail: pawel.michalowski@itme.edu.pl

1 Epitaxial growth of GaN on sapphire

The two-step MOVPE growth of GaN on sapphire was conducted in order to growth high quality epilayers on large lattice mismatch substrate (~16%). The growth process was carried out with an use of trimethylgallium (TMGa) and ammonia (NH_3) as precursors for gallium and nitrogen, respectively, at ~1100°C and 200 mbar. The temperature and growth rate was in situ monitored by Laytec EpiCurve TT system.

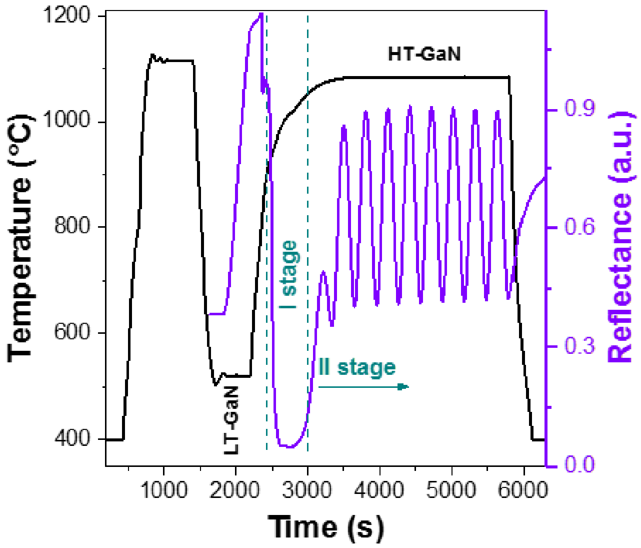

Figure S1: In situ monitoring curves: true temperature (black) and reflectance at 950 nm (violet) for the two-step GaN growth on sapphire.

Figure S1 presents in situ derived curves of true temperature and reflectance measurements for ~1.5 µm-thick GaN epilayer grown on sapphire substrate. Prior to GaN growth, thermal cleaning of the sapphire substrate was carried out at ~1130°C for 10 min. Initially, low-temperature GaN (LT-GaN) was grown at ~520°C, and then temperature was raised to ~1100°C for high-temperature GaN (HT-GaN) growth. HT-GaN growth begins with the I stage (reflectance drop and rise; 3D growth mode), continues with islands coalescence (change from 3D to 2D growth), and then the II stage progresses (2D layer-by-layer growth mode). The region where 2D growth occurs is characterize by uniform thickness oscillations (Fabry-Pérot oscillations), allowing the growth rate determination being ~0.5 nm/s for GaN. The described two-step strained heteroepitaxial growth of GaN (or AlN) with an use of LT buffer layers (either GaN or AlN) was already developed and well documented.[1–4] The growth mechanism was already studied in 1990s, consisting the following steps:[2] i) nucleation of high-density GaN, ii) geometric selection of the crystallographic direction of the GaN fine crystals forming columnar structure, and iii) high lateral growth and coalescence of the trapezoidal island crystals with c-face on top. It was also proven that this two-step growth, in fact the presence of inclined facets of the islands, is a key factor of unintentional dopant incorporation.[5] Additionally, a high density of threading dislocations, $> 10^9 cm^{-2}$, namely edge-type, are formed when island crystals with slight misorientations with respect to each other coalesce.[6]

2 Etch pits evaluation

The etch pits density and their size distribution was evaluated by careful analysis of SEM top view micrographs of etched GaN surface layer, similarly to method described by Knoke et al.,[7] using a grain/particle size analysis protocol. The diameter of etch pits was measured by drawing circle that touches the hexagon at the vertexes using ImageJ software (NIH, USA),[8] considering more than 500 etch pits in typically five randomly chosen SEM micrographs; each image displayed an area of about $4 \times 3\mu m$ with typically between 120 and 150 etch pits. The selection area was drawn manually because automated software was too inaccurate to find all etch pits due to the low contrasts. The area of the section of the etch pits was measured and then its circular equivalent diameter calculated. The relevant steps of etch pits size determination are illustrated in Figure S2: i) filtering of SEM micrograph in order to obtain an image with sharp edges, and ii) manually drawn circle that touches the hexagons at the vertexes prior to size distribution analysis.

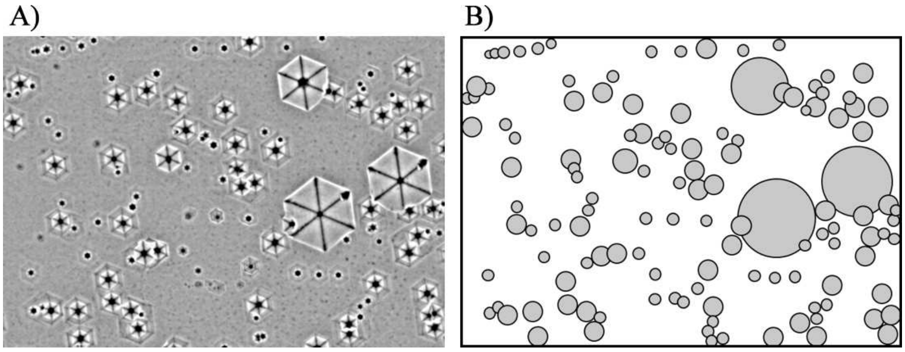

Figure S2: Relevant steps of a protocol of etch pits determination from SEM micrographs. Part A) Filtered SEM micrograph with enhanced quality ($4 \times 3\mu m$). Part B) Manual circle drawing that touches the hexagons at the vertexes corresponding to individual etch pit illustrated in the SEM micrograph.

The obtained size distribution, plotted in Fig. 2 as a representation of normalized frequency histogram of etch pits diameters, shows two clear and narrow maxima, while the distribution of the large etch pits is broader than the latter ones. Then, the maxima were fitted to determine the etch pit size, and the standard deviation was derived from the values measured in the different images.

3 Spatially resolved SIMS

The lateral resolution is mostly determined by the size of the primary beam and thus a smaller beam is preferable. However, in case of 3D imaging it is essential that the primary beam is very homogeneous. Otherwise crater roughness will increase during the experiment and the quality of measurements will decrease with depth. For the SC Ultra tool the ion beam on the sample has a square shape and due to the "variable rectangular shape concept" forms a homogeneous spot. The primary beam at a working point in the SC Ultra is formed by two stencils - well-shaped apertures. While the first one is used to choose the most intense and homogeneous part of the ion beam, the second one changes the size of the spot. This innovation ensures that the resolution will not decrease during the experiment. The drawback is that in practice the smallest size of the spot is about 1 micron. It is possible to image smaller features but in secondary ions image they will inherit the shape and size of the primary beam. As a consequence, the distance between these features should be larger than one micron or they will be blurred together in the secondary ions image.

4 VBC reduction procedure

Figure S3 presents a lateral distribution of oxygen counts in a near-surface area (2D view of the top part of results presented in Fig. 3). The raw data (Part A) contains about 5050 oxygen counts. About 95% of them can be attributed to the VBC. After eliminating random 4800 counts (Part B) it becomes apparant that most oxygen atoms are agglomerated in three structures. Part C presents a similar result but for a sample after a DSE which introduced more oxygen into the system. Rectangular shape of these features can be atributed to the aforementioned SIMS related artifact - secondary ions image of a feature which is much smaller than the primary beam inherits its size and shape.

This simple procedure is not flawless as it may reduce a count which comes from a agglomerated oxygen and leave a count which should be reduced but it is effective enough to show that most oxygen atoms are agglomerated along pillar-shaped structures.

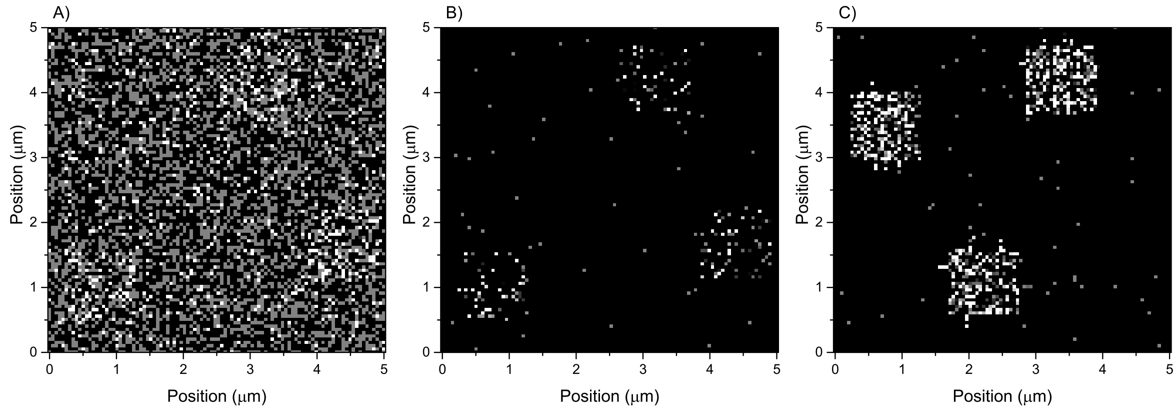

Figure S3: Lateral distribution of oxygen counts in a near-surface area. Part A: raw data, Part B: background contribution subtracted. Part C: similar result for a sample after a DSE.

References

[1] Shuji Nakamura. GaN growth using GaN buffer layer. *Japanese Journal of Applied Physics*, 30:L1705–L1707, 1991.

[2] K. Hiramatsu, S. Itoh, H. Amano, I. Akasaki, N. Kuwano, T. Shiraishi, and K. Oki. Growth mechanism of GaN grown on sapphire with AlN buffer layer by MOVPE. *Journal of Crystal Growth*, 115(1):628 – 633, 1991.

[3] Ismail Altuntas, Ilkay Demir, Ahmet Emre Kasapoğlu, Soheil Mobtakeri, Emre Gr, and Sezai Elagoz. The effects of two-stage HT-GaN growth with different V/III ratios during 3D-2D transition. *Journal of Physics D: Applied Physics*, 51(3):035105, 2017.

[4] Xiaojuan Sun, Dabing Li, Yiren Chen, Hang Song, Hong Jiang, Zhiming Li, Guoqing Miao, and Zhiwei Zhang. In situ observation of two-step growth of AlN on sapphire using high-temperature metalorganic chemical vapour deposition. *CrystEngComm*, 15:6066–6073, 2013.

[5] R.A. Oliver. Application of highly silicon-doped marker layers in the investigation of unintentional doping in GaN on sapphire. *Ultramicroscopy*, 111(1):73 – 78, 2010.

[6] X. J. Ning, F. R. Chien, P. Pirouz, J. W. Yang, and M. Asif Khan. Growth defects in GaN films on sapphire: The probable origin of threading dislocations. *Journal of Materials Research*, 11(3):580592, 1996.

[7] I.Y. Knoke, P. Berwian, E. Meissner, J. Friedrich, H.P. Strunk, and G. Mller. Selective etching of dislocations in GaN grown by low-pressure solution growth. *Journal of Crystal Growth*, 312(20):3040 – 3045, 2010.

[8] Caroline A. Schneider, Wayne S. Rasband, and Kevin W. Eliceiri. NIH Image to ImageJ: 25 years of image analysis. *Nature Methods*, 9:671, 2012.